Node-to-node field calibration of wireless distributed air pollution sensor network[☆]

Fadi Kizel [a], Yael Etzion [a], Rakefet Shafran-Nathan [a], Ilan Levy [a], Barak Fishbain [a], Alena Bartonova [b], David M. Broday [a, *]

[a] Faculty of Civil and Environmental Engineering, Technion - Israel Institute of Technology, Haifa 32000, Israel
[b] Norwegian Institute for Air Research (NILU), Kjeller, Norway

ABSTRACT

Low-cost air quality sensors offer high-resolution spatiotemporal measurements that can be used for air resources management and exposure estimation. Yet, such sensors require frequent calibration to provide reliable data, since even after a laboratory calibration they might not report correct values when they are deployed in the field, due to interference with other pollutants, as a result of sensitivity to environmental conditions and due to sensor aging and drift. Field calibration has been suggested as a means for overcoming these limitations, with the common strategy involving periodical collocations of the sensors at an air quality monitoring station. However, the cost and complexity involved in relocating numerous sensor nodes back and forth, and the loss of data during the repeated calibration periods make this strategy inefficient. This work examines an alternative approach, a node-to-node (N2N) calibration, where only one sensor in each chain is directly calibrated against the reference measurements and the rest of the sensors are calibrated sequentially one against the other while they are deployed and collocated in pairs. The calibration can be performed multiple times as a routine procedure. This procedure minimizes the total number of sensor relocations, and enables calibration while simultaneously collecting data at the deployment sites. We studied N2N chain calibration and the propagation of the calibration error analytically, computationally and experimentally. The *in-situ* N2N calibration is shown to be generic and applicable for different pollutants, sensing technologies, sensor platforms, chain lengths, and sensor order within the chain. In particular, we show that chain calibration of three nodes, each calibrated for a week, propagate calibration errors that are similar to those found in direct field calibration. Hence, N2N calibration is shown to be suitable for calibration of distributed sensor networks.

© 2017 Elsevier Ltd. All rights reserved.

1. Introduction

Air pollution is known to levy severe health effects and high risks for the public (World Health Organization, 2013; Crouse et al., 2012; Lepeule et al., 2012), hence air quality is regularly monitored in many regions worldwide. Regulatory air pollution monitoring is mainly performed by stationary and routinely calibrated reference Air Quality Monitoring (AQM) instruments, which measure the concentrations of different criteria pollutants, typically ozone (O_3),

nitrogen oxides (NO_x), carbon monoxide (CO), sulfur dioxide (SO_2), and particulate matter (PM). While AQM stations provide reliable and accurate measurements, they are expensive to install and to operate, and require professional maintenance and personnel. Therefore, the spatial distribution of AQM stations is rather sparse. The use of geospatial interpolation or regression methods for estimating ambient concentrations of (and exposure to) monitored pollutants away from the AQM stations is a common procedure for bridging over the sparse spatial availability of the observations (Yuval and Broday, 2006; Eitan et al., 2010; Whitworth et al., 2011; Myers et al., 2013; Sampson et al., 2013). Yet, such a mapping is significantly affected by the spatial distribution of the stations (Yuval and Broday, 2006) and the temporal resolution of the reported data, and may involve spatially biased model errors (Yuval et al., 2017). Such model errors tend to propagate when concentration maps are used for, e.g., exposure estimation, in particular in

areas that are characterized by considerable spatiotemporal concentration variability (Yuval et al., 2017; Zandbergen et al., 2012; O'Leary and Lemke, 2014; Reggente et al., 2015).

Recently, miniaturization of sensor technology has enabled deployment of multi-sensor Micro Sensing Units (MSUs, hereinafter nodes) as part of Wireless Distributed Sensor Networks (WDSNs) for air quality measurements (Kumar et al., 2015; Kotsev et al., 2016; Mead et al., 2013; Moltchanov et al., 2015). Dense deployment of such sensor nodes can capture the spatiotemporal variability of urban air pollution and provide more reliable exposure and risk estimates. Yet, these sensors have limited accuracy (Moltchanov et al., 2015), tendency to degrade and age relatively fast (De Vito et al., 2008; Saukh et al., 2015), and they suffer from severe interference by co-existing airborne pollutants and meteorological parameters (Fishbain et al., 2017; Castell et al., 2017). Many of these limitations are normally unaccounted for during lab testing and calibration, which are performed in controlled chambers (Mead et al., 2013; Castell et al., 2017; Williams et al., 2013). These limitations call for frequent field calibrations under real environmental conditions, to assure reliable measurements.

Field calibration of WDSN sensors has been studied using the so-called collocation procedure, where the nodes are placed next to a standard AQM station and the time series recorded by the sensors are regressed against the co-measured AQM data (Mead et al., 2013; Moltchanov et al., 2015; Fishbain et al., 2017; Castell et al., 2017; Williams et al., 2013; Holstius et al., 2014; Deary et al., 2016; Spinelle et al., 2015; Jiao et al., 2016). Specifically, this approach relies on placing the sensor next to a reference device for a certain time-period, averaging the rich sensor data to fit the lower sampling frequency of the reference device, and performing a pairwise linear-regression between the sensor and the AQM datasets. The regression coefficients are then used to correct the sensor measurements and make them follow the reference data.

Let $\mathbf{y}$ and $\mathbf{x}$ be the registered measurements by the reference device and by the WDSN sensor, respectively. Assuming a linear relationship between $\mathbf{y}$ and $\mathbf{x}$ (Moltchanov et al., 2015; Spinelle et al., 2015),

$$\mathbf{y} = \alpha \cdot \mathbf{x} + \beta + \mathbf{e}, \tag{1}$$

where α and β are the slope and intercept of the linear model, respectively, and $\mathbf{e}$ is a vector of the model errors, which are assumed to have a zero mean. Let $\hat{\alpha}$ and $\hat{\beta}$ be the estimated coefficients that are obtained using the collocation data. The calibrated measurements, $\hat{\mathbf{x}}$, are given by:

$$\hat{\mathbf{x}} = \hat{\alpha} \cdot \mathbf{x} + \hat{\beta}. \tag{2}$$

It is noteworthy that the length of the collocation period in which the sensors are adjacent to the AQM station until a reliable calibration is obtained may vary, depending on the environmental conditions (Moltchanov et al., 2015; Saukh et al., 2015; Balzano and Nowak, 2007; Hasenfratz et al., 2012) and the sensor technology (Williams et al., 2013; Holstius et al., 2014). Moreover, relocating the sensor nodes to the AQM station for calibration is labor intensive, and for a WDSN with a large number of nodes can become cumbersome. Frequent relocations of nodes to the AQM station for calibration involve also loss of measurements until the sensors are returned to their prescribed deployment sites. As such, this strategy counteracts the main advantage of the WDSN concept − richness and continuous data.

A field calibration procedure that does not require collocation at an AQM station has been suggested (Fishbain and Moreno-Centeno, 2016) for cases where the measurement errors comply with certain limitations. Yet, since the sensors are calibrated against the mean reading of all the reporting WDSN nodes, they may still provide values that do not conform with those measured by a reference device. For example, if all the sensors have a systematic measurement error this method will come short of reporting accurate concentrations (Moltchanov et al., 2015).

We propose here an alternative strategy, designated node-to-node (N2N) calibration. The idea is to employ chain calibration of the sensors in the field, with minimal interruption to the continuous measurement and fewer hops of the nodes between their deployment sites and the reference (AQM) site. Whereas N2N calibration is not limited to stationary nodes, for simplicity we assume in the following WDSNs with stationary nodes. WDSN sensors require proactive frequent calibrations, therefore a calibration procedure that involves a smaller number of collocations at AQM stations is advantageous as it enables versatile calibration logistics. Moreover, continuous measurement at the deployment sites guarantees little missing data and better spatial and temporal analyses. Reducing the number of collocations is also cost effective and environmental friendly, since WDSNs may be deployed quite far from AQM stations, i.e. the nodes may be closer to each other than to a distant AQM station.

Let $\text{AQM} \leftarrow u_1 \leftarrow u_2 \leftarrow u_3 \leftarrow \cdots \leftarrow u_{n-1} \leftarrow u_n$ represent a sequence of collocated nodes, such that sensor u_1 is collocated next to an AQM instrument for a period T. Then it is relocated and collocated with sensor u_2 (during a non-overlapping period T). Next, sensor u_2 is relocated and collocated with sensor u_3 (during a non-overlapping period T), etc. Finally, the last sensor u_n is collocated next to sensor u_{n-1}. At this stage, sensor u_n can be N2N calibrated against the AQM data. Yet, the process can end also by relocating sensor u_n to the AQM station, such that the N2N calibration process can be evaluated. Namely, the N2N calibration procedure proposes that all the sensors $\{u_1, u_2, \cdots, u_n\}$ are calibrated one against the other in a sequential manner, with all of them (but u_1) not collocated at the AQM station. In fact, N2N calibration has been suggested before but its mathematical model for stationary nodes was developed only for two sequential sensor pairings (Hasenfratz et al., 2012; Bychkovskiy et al., 2003). Similarly, N2N calibration of mobile sensors was also suggested by pairing events, inherent for roaming sensors mounted on vehicles (Saukh et al., 2015), using Geometric Mean Regression (GMR) to reduce the propagation of the calibration error relative to Ordinary Least Squares (OLS) regression. However, the study accounted only for the slope and disregarded the effect of the intercept on the accumulated calibration error.

Here, we study N2N calibration of stationary sensors both analytically, computationally, and experimentally, demonstrating the effect of the number and order of the nodes on the propagation of calibration coefficient errors (slope and intercept) and the overall calibration uncertainty. We present a detailed derivation of chain calibration equations and of the respective error propagation, followed by computational results that confirm the analytical derivation and reveal certain limitations of the process. Next, experimental results of WDSN nodes that were first collocated at an AQM station and then deployed in the field are presented, and the N2N calibration process and the propagation of calibration errors throughout the network are demonstrated. We conclude by discussing the suitability of the method for field calibration of air quality WDSNs.

2. Methods

2.1. Theoretical aspects of node-to-node calibration

Let sensor u_1 be collocated next to an AQM reference device for a time-period T_1 and let sensor u_2 be collocated next to sensor u_1 for
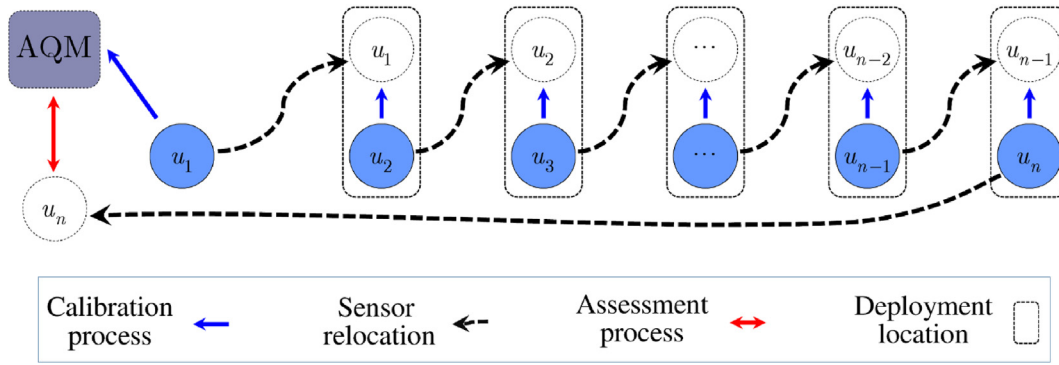
Fig. 1. Schematic representation of the N2N calibration process. In blue are the sensors' initial deployment locations. Black dashed arrows represent sequential relocations of the sensor nodes, with time progressing from left to right and with each dashed line representing a non-overlapping period of T days (for practical reason, $T_i \equiv T$). Blue arrows represent node-to-AQM or N2N calibrations, with time progressing from left to right and with each arrow representing a new calibration period. Collocation sites are designated by boxes. The double headed red arrow represents the first T-days period following the current $n \cdot T$ days sequence length, where both evaluation of the N2N calibration and analysis of the propagation of the calibration errors can be performed, and correction measures can be applied by re-calibrating the nth sensor. This sensor serves as the first calibrated sensor in a new calibration sequence. (For interpretation of the references to colour in this figure legend, the reader is referred to the web version of this article).

a consecutive time-period T_2 that does not overlap with T_1 (Fig. 1). Assuming linear relationships between the sensors' and the AQM station data, the N2N calibration process implies that for any pollutant we can obtain the calibrated measurements, $\hat{\mathbf{x}}_2$, of sensor u_2 by applying Eq. (2) sequentially. Namely, by performing a sequence of sensor-to-sensor calibration we can first obtain $\hat{\mathbf{x}}_{AQM \leftarrow 1}$, i.e. calibration of the raw data from sensor u_1 against the reference AQM data,

$$\hat{\mathbf{x}}_{AQM \leftarrow 1} = \hat{\alpha}_1 \cdot \mathbf{x}_1 + \hat{\beta}_1, \tag{3}$$

and then use the calibrated sensor to indirectly calibrate sensor u_2 to the reference AQM records, by calibrating it to u_1 while they are collocated,

$$\hat{\mathbf{x}}_2 = \hat{\alpha}_1 \cdot \hat{\mathbf{x}}_{1 \leftarrow 2} + \hat{\beta}_1 = \hat{\alpha}_1 \cdot \left(\hat{\alpha}_2 \cdot \mathbf{x}_2 + \hat{\beta}_2 \right) + \hat{\beta}_1$$
$$= \left(\hat{\alpha}_1 \cdot \hat{\alpha}_2 \right) \cdot \mathbf{x}_2 + \left(\hat{\alpha}_1 \cdot \hat{\beta}_2 + \hat{\beta}_1 \right). \tag{4}$$

Clearly, a similar chain calibration can be applied for longer sensor sequences. For example, for a chain of three sensors that are calibrated against each other during non-overlapping time-periods with only one sensor collocated next to a reference device, the equivalent expression is

$$\hat{\mathbf{x}}_3 = \hat{\alpha}_1 \left(\hat{\alpha}_2 \left(\hat{\alpha}_3 \, \mathbf{x}_3 + \hat{\beta}_3 \right) + \hat{\beta}_2 \right) + \hat{\beta}_1$$
$$= \left(\hat{\alpha}_1 \cdot \hat{\alpha}_2 \cdot \hat{\alpha}_3 \right) \mathbf{x}_3 + \left(\hat{\alpha}_1 \cdot \hat{\alpha}_2 \cdot \hat{\beta}_3 + \hat{\alpha}_1 \cdot \hat{\beta}_2 + \hat{\beta}_1 \right). \tag{5}$$

This expression can be easily generalized to a sequence of n sensors in a row, with the calibrated measurements of the nth sensor, $\hat{\mathbf{x}}_n$, being

$$\hat{\mathbf{x}}_n = \left(\prod_{i=1}^{n} \hat{\alpha}_i \right) \cdot \mathbf{x}_n + \sum_{j=2}^{n} \left(\left(\prod_{i=1}^{j-1} \hat{\alpha}_i \right) \cdot \hat{\beta}_j \right) + \hat{\beta}_1. \tag{6}$$

Due to the linear nature of the process, Eq. (6) reveals that the order of the sensors in the calibration sequence is unimportant. In a more concise writing, the linear regression of u_n against the AQM data can be written as

$$\hat{\mathbf{x}}_n = \hat{\alpha}_{AQM \leftarrow n} \cdot \mathbf{x}_n + \hat{\beta}_{AQM \leftarrow n}, \tag{7}$$

where

$$\hat{\alpha}_{AQM \leftarrow n} = \prod_{i=1}^{n} \hat{\alpha}_i, \tag{8}$$

and

$$\hat{\beta}_{AQM \leftarrow n} = \sum_{j=2}^{n} \left(\left(\prod_{i=1}^{j-1} \hat{\alpha}_i \right) \cdot \hat{\beta}_j \right) + \hat{\beta}_1. \tag{9}$$

It is noteworthy that $\hat{\alpha}_{AQM \leftarrow n}$ depends on all the estimated sensor-to-sensor regression slopes, $\hat{\alpha}_i$, and that the intercept $\hat{\beta}_{AQM \leftarrow n}$, is affected both by the slopes, $\hat{\alpha}_i$, (except for $\hat{\alpha}_n$) and the intercepts, $\hat{\beta}_i$. Consequently, the estimation errors of the regression co-efficients of each sensor in the calibration chain propagate throughout the N2N calibration procedure and accumulate in the overall calibration error. Yet, as will be demonstrated, by carefully tracking the propagation of the calibration errors throughout the N2N calibration it may be possible to detect the failure of specific sensors.

2.2. Error propagation in N2N calibration

Let $s^2_{\hat{\alpha}_i}$, $s^2_{\hat{\beta}_i}$, and $s_{\hat{\alpha}_i \hat{\beta}_i}$ be the variance and covariance of the calibration coefficients $\hat{\alpha}_i$ and $\hat{\beta}_i$ between sensors u_i and u_{i-1} (where u_0 is the reference AQM sensor). For simplicity, we designate $\hat{\alpha} = \hat{\alpha}_{AQM \leftarrow n}$ and $\hat{\beta} = \hat{\beta}_{AQM \leftarrow n}$. According to the error propagation theorem (Taylor, 1997), the errors of these calibration coefficients are given by

$$s_{\hat{\alpha}} = \sqrt{\sum_{i=1}^{n} \left(\frac{\partial \hat{\alpha}}{\partial \hat{\alpha}_i} \right)^2 s^2_{\hat{\alpha}_i} + \sum_{i=1}^{n} \left(\frac{\partial \hat{\alpha}}{\partial \hat{\beta}_i} \right)^2 s^2_{\hat{\beta}_i} + \sum_{i=1}^{n} \left(\frac{\partial \hat{\alpha}}{\partial \hat{\alpha}_i} \cdot \frac{\partial \hat{\alpha}}{\partial \hat{\beta}_i} \, s_{\hat{\alpha}_i \hat{\beta}_i} \right)}, \tag{10}$$

$$s_{\hat{\beta}} = \sqrt{\sum_{i=1}^{n}\left(\frac{\partial\hat{\beta}}{\partial\hat{\alpha}_i}\right)^2 s_{\hat{\alpha}_i}^2 + \sum_{i=1}^{n}\left(\frac{\partial\hat{\beta}}{\partial\hat{\beta}_i}\right)^2 s_{\hat{\beta}_i}^2 + \sum_{i=1}^{n}\left(\frac{\partial\hat{\beta}}{\partial\hat{\alpha}_i}\cdot\frac{\partial\hat{\beta}}{\partial\hat{\beta}_i}\ s_{\hat{\alpha}_i\hat{\beta}_i}\right)},$$

(11)

Using Eqs. (8) and (9) for calculating the partial derivatives of $\hat{\alpha}$ and $\hat{\beta}$ (see details in the electronic Supporting Information) and assuming that they are uncorrelated (e.g. $s_{\hat{\alpha}_i\hat{\beta}_i} = 0$, see justification below), the calibration error of any measurement by sensor u_n, i.e. which accompanies Eq. (7), is

$$s_{\hat{x}_n} = \sqrt{\left(\frac{\partial\hat{x}_n}{\partial\hat{\alpha}}\right)^2 s_{\hat{\alpha}}^2 + \left(\frac{\partial\hat{x}_n}{\partial\hat{\beta}}\right)^2 s_{\hat{\beta}}^2} = \sqrt{x_n^2 s_{\hat{\alpha}}^2 + s_{\hat{\beta}}^2},$$

(12)

where x_n is an element of $\mathbf{x}_n$. The normalized calibration error is

$$\widetilde{s}_{\hat{x}_n} = \frac{s_{\hat{x}_n}}{x_n} = \sqrt{\frac{x_n^2 s_{\hat{\alpha}}^2 + s_{\hat{\beta}}^2}{x_n^2}} = \sqrt{s_{\hat{\alpha}}^2 + \frac{s_{\hat{\beta}}^2}{x_n^2}}.$$

(13)

Due to having x_n^2 in the denominator of Eq. (13), the normalized calibration error has a lower bound ($\lim_{x_n\to\infty} \widetilde{s}_{\hat{\mathbf{x}}_n} = s_{\hat{\alpha}}$) but it is unbounded for very low x_n. Thus, in general, low measurements (x_n) are expected to show higher normalized calibration errors. Moreover, Eqs. (10—13) suggest that the overall calibration error increases with the length of the calibration sequence.

2.3. Computational calculation of the propagation of calibration errors

To examine the theoretical predictions (Eq. (13)), we used half hourly O_3 concentrations measured during 14 days in winter 2014 by 16 collocated sensor nodes (Elm, Perkin Elmer, USA; see sensor specifications in the SI), and calculated the linear regression coefficients between each pair of sensors (120 pairs in total). The negligible mean covariance between the slope and the intercept, $\overline{s_{\hat{\alpha}_i\hat{\beta}_i}} = -0.04\pm0.03$, supports our assumption to ignore it in Eq. (12). Starting with a single pair of sensors (i.e. a chain length of one), we simulated adding one sensor at a time and generating sensor sequences of increasing lengths, from one and up to 20 sensors. To simulate the N2N calibration process, the sensor sequence was developed by drawing a random pair from all the permissible possibilities, accounting for the last sensor that has been added but allowing the use of sensors more than once throughout the calibration process (as will be demonstrated in the field study, Fig. S1). To avoid a possible selection bias, construction of the calibration chains was repeated 10 times, creating 10 different sequences for each sensor-chain length. The regression coefficients between each pair in the sequence were used for calculating the normalized calibration error, Eq. (13), as sensors were added to the chains.

As derived theoretically, the normalized calibration error is larger for lower concentrations, x_n, regardless of the sensor sequence length, and it increases with the sensor sequence length (Fig. 2) and can attain large values for long chains. However, this can be circumvented by avoiding long calibration chains and/or by using better sensors (e.g. super-nodes), since the rate at which the calibration errors accumulate depend on the performance of individual sensors. In general, more accurate sensors enable maintaining longer calibration chains before the error exceeds a preset threshold.
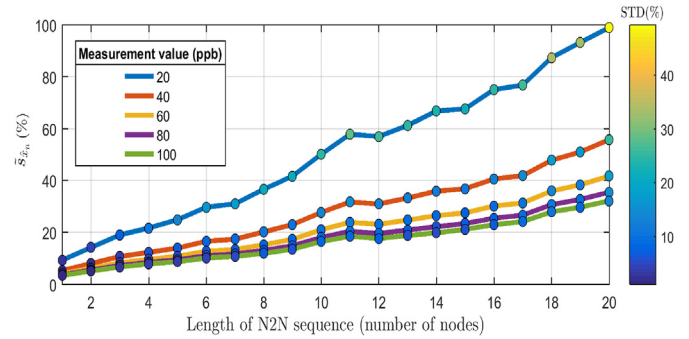

Fig. 2. Normalized calibration errors (Eq. (13)) of N2N calibration as a function of the length of the sensor sequence. The curves represent average results of 10 chains for which the concentration reported by the last sensor to be added, x_n, is as noted. The color of the dots represents the STD of the 10 chains (of the same length and x_n). (For interpretation of the references to colour in this figure legend, the reader is referred to the web version of this article).

3. Experimental design

3.1. Study area

To evaluate the N2N calibration procedure (Fig. 1), air quality measurements were conducted in the Neve Shaanan neighborhood and at the Atzmaut downtown area of the Mediterranean coastal city of Haifa, Israel (Fig. 3). Collocation measurements were performed at two AQM stations, located in two different yet typical urban microenvironments. The Neve Shaanan (NSH) AQM station is located in a planar residential area on the northeastern slop of Mount Carmel, about 200 m a.s.l. A major road crosses the neighborhood and connects the northeastern and southwestern slopes of the Carmel Ridge, passing through the Ziv junction - a small yet busy neighborhood commercial area. The mean traffic volume in the neighborhood during the day ranges from 300 vehicles h^{-1} in quiet roads and up to 2000 vehicles h^{-1} in the neighborhood main artery. The Atzmaut (ATZ) AQM station is a roadside (e.g. transportation affected) site, located in a downtown commercial area near the Haifa harbor and train station. The mean daytime traffic volume in its vicinity is ~3000 vehicles h^{-1}.

3.2. Sensor technologies

Two ambient pollutants were studied: NO (a primary pollutant emitted in urban areas mainly by traffic) and O_3 (a secondary pollutant). The measurements of these pollutants were performed by distinct sensor technologies and platforms. Namely, ambient O_3 concentrations were measured using metal oxide (MO) sensors (Aeroqual, New Zealand) mounted in Elm nodes (Perkin Elmer, USA) (Moltchanov et al., 2015) whereas NO concentrations were measured using electrochemical (EC) sensors (AlphaSense, UK) mounted in AQMesh pods (Geotech, UK) (Mead et al., 2013) (see the SI for additional sensor specifications). Data were recorded every 30 min (O_3) and 15 min (NO) by the two WDSN arrays (Table 1).

3.3. Calibration period

It has been shown (Moltchanov et al., 2015) that convergence of the estimated regression coefficients requires a minimum calibration period. Let t_c be the number of collocation days needed until convergence of the calibration coefficients is attained, T be the actual number of days of sensor collocations, and τ be the number of days a sensor can operate reliably between consecutive calibrations. Assuming t_c and τ to be constant (i.e. not to change from
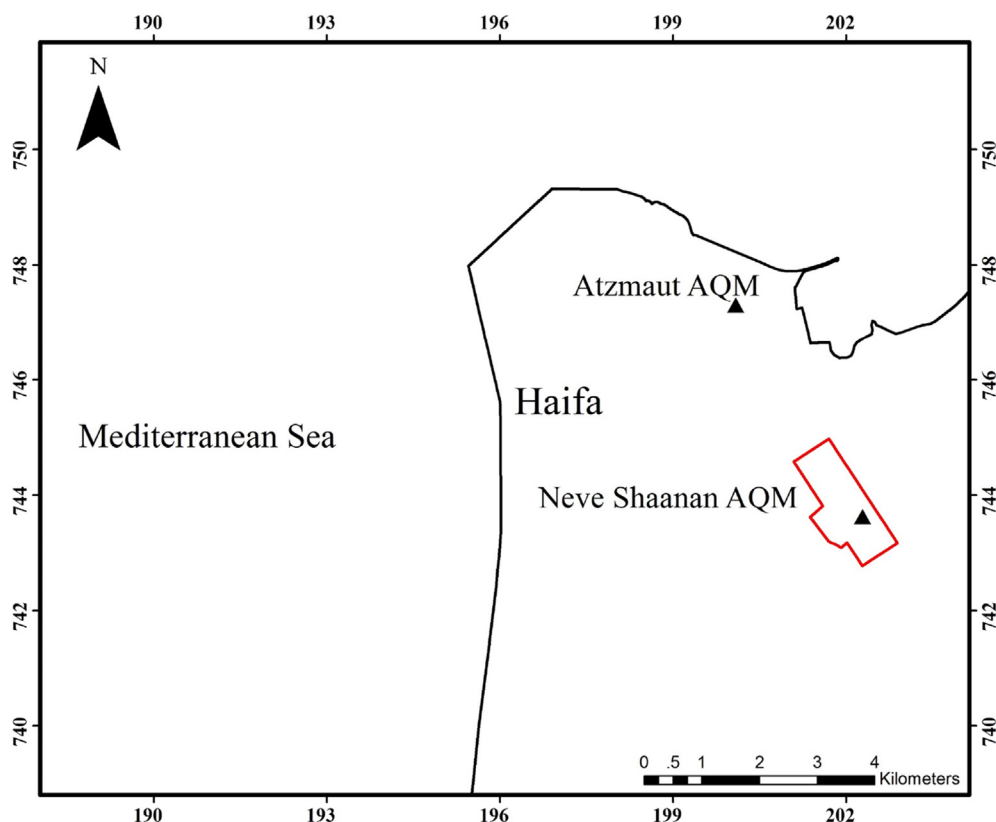
Fig. 3. Study area, with the Neve Shaanan and Atzmaut AQM stations (marked by triangles) and the Neve Shaanan neighborhood (marked by a red polygon). (For interpretation of the references to colour in this figure legend, the reader is referred to the web version of this article).

Table 1
Details of the collocation campaigns.

Experiment[a]	Pollutant	Sensor type & platform[b]	Sensor ID	AQM station	Collocation period
Set 1	O_3	MO (PE)	414, 422, 624, 626	Neve Shaanan	(29/04/14)–(28/05/14)
Set 2	O_3	MO (PE)	418, 621, 620	Neve Shaanan	(09/06/14)–(10/07/14)
Set 3	NO	EC (GT)	135, 136, 468	Atzmaut	(03/02/15)–(26/02/15)
Set 4	NO	EC (GT)	220, 465, 471	Atzmaut	(27/02/15)–(28/04/15)

[a] Sensor data in Sets 1 & 2 were re-sampled from the original time resolution (15 min) to the AQM time resolution (30 min). AQM data in Sets 3 & 4 were re-sampled from the original time resolution (5 min) to the sensor time resolution (15 min).
[b] MO − metal oxide, EC − electrochemical, PE - Perkin Elmer (USA), GT − Geotech (UK).

collocation to collocation or among seasons), the N2N calibration (Fig. 1) can be applied for a sequence length of $n = \tau/T$ sensors before re-collocation at the AQM station of one of the nodes. Both τ and t_c are sensor characteristics that depend on the quality of the sensors and their sensitivity to the measurement conditions (physical environment, meteorology, etc.) (Moltchanov et al., 2015; Fishbain et al., 2017; Castell et al., 2017). On the other hand, T can be arbitrary as long as $T \geq t_c$. Clearly, smaller T values enable longer chain sequences, n. It is noteworthy that according to the N2N calibration scheme (Fig. 1), each sensor is relocated and calibrated only once in τ days. Moreover, applying a continuous N2N calibration, each sensor will be eventually collocated at the AQM station once in $n \cdot \tau$ days (for a period of T days) and directly calibrated against data collected by the AQM reference instrument. Since τ depends on the sensor technology and environmental conditions, it must be carefully assessed as part of the calibration scheme. Based on our previous work (Moltchanov et al., 2015; Castell et al., 2017), a conservative estimate of τ for both the O_3 and NO sensors used in this study is six weeks (based on continuous sensor monitoring for up to five months and accounting solely for sensor aging).

The minimum number of collocation days needed for reliable

calibration of a given sensor type, t_c, was determined based on the convergence of the calibration coefficients and of the regression goodness of fit (coefficient of determination, R^2 (Crouse et al., 2012)). We calculated the linear regression (Eq. (2)) based on an increasing number of records, taking 24 h (i.e. daily) incremental steps as practical time steps of a field calibration procedure. Specifically, each additional calibration day added 48 (O_3) or 96 (NO) data points. The actual number of collocation days for a given sensor type, T, was set as the fixed (protocol) period for field calibration of all the sensors of this type throughout the study, both against the reference AQM device and against each other. Due to practical reasons, we applied a common T that was suitable for both sensor technologies, as explained below. Initially, all the sensor nodes were collocated at the AQM stations (Table 1), enabling easy assessment of the required calibration period.

3.4. N2N chain calibration

N2N chain calibration was studied using two experimental designs: with the nodes collocated solely at the two AQM stations and while they were deployed as an operative WDSN in the Neve

Shaanan study area. In the former, we used data from Sets 1–4 (Table 1), where the sensors were next to the NSH or AZT AQM stations. Two scenarios were examined for each Set, with the same sensor in each scenario calibrated using three sensor chains (sequences) of different lengths: a direct calibration of the sensor against the AQM device and indirect calibration through one or two intermediate sensors. Based on our results, we set the number of collocation days used for calibration, T, for both sensor-to-AQM and sensor-to-sensor for one week. The calibration error was calculated for each of the above sequences by comparing the calibrated data of the last sensor in the chain against the AQM reference data, using records that were not used for the N2N calibration. This design enabled us to compare direct calibration and N2N calibration under identical environmental conditions and time-periods, i.e. with minimal uncertainty. Moreover, this design enabled evaluation of N2N calibration for a varying length of the sensor chains, and thus to compare the actual propagation of the calibration errors with the computational predictions (Fig. 2).

In the second experimental design, we tested N2N calibration under real deployment conditions against data from an AQM reference device, using five Elm nodes deployed across the Neve Shaanan neighborhood, Haifa, between 29/4–29/7, 2014 (with only one node initially collocated at the AQM station, Fig. 1 and Fig. S1). The dynamic deployment plan of the O_3 sensors enabled us to study two N2N calibration sequences (see SI and Fig. S1). Data collected by the last sensor in the sequence were calibrated by means of the N2N calibration procedure (Eq. (6)) and compared to the measurements of the AQM device, such that the performance of the N2N calibration process could be assessed. In addition, the measurements of this sensor passed also an independent (i.e. direct) calibration against the AQM data (Eq. (2)), enabling the onset of a new N2N calibration chain with this node as the first node. To evaluate the accuracy and precision of N2N calibration we examined the residuals $\varepsilon_{\hat{\mathbf{x}}}$,

$$\varepsilon_{\hat{\mathbf{x}}} = \hat{\mathbf{x}} - \mathbf{y}, \tag{14}$$

and the normalized calibration error, $\varepsilon_{\hat{\mathbf{x}}}(k)/\mathbf{y}(k)$, of data points that were not used for calibration. The statistics used for evaluating the N2N calibration are detailed in the electronic Supporting Information.

4. Results and discussion

4.1. Calibration period

Data from Sets 1–4 (Table 1) were used for determining the required collocation period, based on the convergence of $\hat{\alpha}$, $\hat{\beta}$ and R (Crouse et al., 2012) against the calibration period length (Figs. S2 and S3). For the O_3 sensors, convergence of R^2 is apparent after seven days whereas for the NO sensors, convergence of R^2 is apparent after two days. As seen, the convergence of the slope, $\hat{\alpha}$, is faster than that of the intercept, $\hat{\beta}$. It is also noteworthy that the slope of O_3 sensor 626 (Set 1, Fig. S2) drifted over time due to the sensor being faulty and not due to a change in the environmental conditions, as the other sensors did not show a similar pattern. Based on these results, the sensors' operational calibration duration, T, was set to be one week for all the sensors (this decision reflects, in part, practical and convenience considerations). This calibration duration applied for both direct calibration of the sensors against the AQM device and the N2N (sensor-to-sensor) calibration.

4.2. Individual sensor performance

Fig. 4 and Fig. S4 depict scatter plots of directly calibrated ($\hat{\mathbf{x}}$) and AQM ($\mathbf{y}$) measurements, and histograms of the normalized calibration errors. Apart from O_3 sensor 626 (Set 1), all the sensors showed an almost zero mean calibration error. Since the mean absolute error (MAE) of sensor 626 ($MAE_{626} = 5$ ppb) was higher than the average MAE of the other O_3 sensors in Set 1 ($\overline{MAE} = 2.7$ ppb) while its standard deviation ($SD_{MAE, 626} = 4.1$ ppb) was similar to the average SD_{MAE} of the other sensors in Set 1 ($\overline{SD}_{MAE} = 3.5$ ppb), sensor 626 is clearly inaccurate, as was already noted. This analysis shows how a careful examination of the WDSN data can be used to identify faulty sensors and, therefore, to reduce the propagation of measurement errors throughout the N2N calibration process, by avoiding their use.

As a contrary example, measured NO concentrations in Set 4 ranged between zero and about 500 ppb (Fig. S4) and showed a considerably higher standard deviation than in Set 3 (Fig. 4). However, the average of the mean absolute normalized error, which is blind to the magnitude of the measurement, is similar for Sets 3 and 4 ($\overline{MAnE} = 26\%$ and 21.3%, respectively), and the $\overline{SD}_{MAnE}$ of these sets is 35% and 30%, respectively. Hence, it seems that the NO sensors performed well during Set 4 measurements and that the higher NO concentrations measured in Set 4 (0–500 ppb) relative to Set 3 (0–300 ppb) were reliable.

Thus, we demonstrated for two pollutants (O_3 and NO), two sensor technologies (MO and EC) and two platforms (Elm and AQMesh) that pooled analysis of calibrated sensor data, collected by relatively low-cost sensors under common ambient pollutant levels, can be used for assessing the reliability and performance of individual sensors.

4.3. Sensor calibration stability

Without continuous calibration the quality of the concentrations reported by the sensors will quickly deteriorate, deeming the WDSN untrusty. In particular, use of erroneous sensor data for air resources management, environmental epidemiology studies, or citizen engagement may bias the estimated exposure and/or raise unwarranted public concerns. For a calibration procedure to be effective, it should be stable for long time-periods, thus avoiding the need for a frequent calibration duty-cycle. In practice, however, the stability of the calibration coefficients is limited and they may change due to varying environmental conditions (Moltchanov et al., 2015; Saukh et al., 2015; Fishbain et al., 2017; Castell et al., 2017; Spinelle et al., 2015). In fact, calibration consistency is a problem also of standard monitoring equipment, and AQM operation guidelines respond to this by requiring frequent automated checks of the monitoring equipment. For example, the USEPA guidelines require that Level 1 zero and span checks will be performed every two weeks, and AQM stations in Israel do this automatically on a weekly basis. Similarly, detection of changes in the sensor calibration coefficients can be achieved by regular surveillance of the records, as part of a quality assurance/quality control procedure.

Here, we report the stability of the calibration coefficients of four sensors that have been collocated next to an AQM station for a week (time period I), deployed in another location (time period II), and then re-collocated at the same AQM station for yet two more weeks (time period III) (Table 2). Calibration coefficients for each sensor were estimated based on measurements from the first period and from the first week of the third period. The two sets of calibration coefficients were applied to raw measurements from the second week of period III, and the calibrated records were evaluated against the AQM measurements from this period. Fig. S5 depicts scatter plots of the pre-calibrated and the calibrated
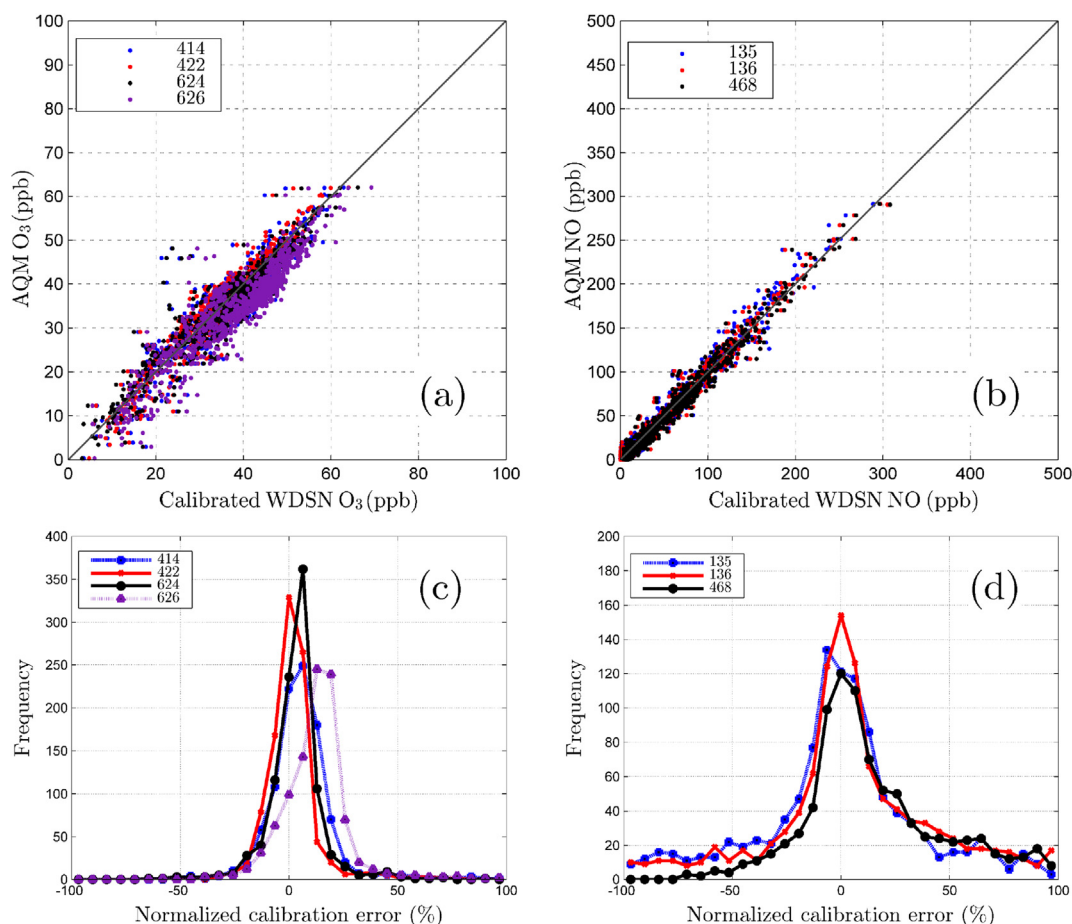
Fig. 4. Scatter plots of directly calibrated O_3 measurements by the Elm nodes (Set 1) against Neve Shaanan AQM O_3 data (a), and of directly calibrated NO measurements by the AQMesh nodes (Set 3) against Atzmaut AQM NO data (b). The lower row presents the corresponding histograms of the normalized calibration errors for O_3 (c) and NO (d).

Table 2
Mean absolute error (MAE) and mean absolute normalized error (MAnE) of calibrated O_3 sensor measurements and AQM data from the second week of period III (16—22/7, 2014), based on calibrations using measurements from period I (22/5—28/5, 2014) or from the first week of period III (9—15/7, 2014).

Sensor no.	MAE (ppb)		MAnE (%)	
	Calibration based on collocation in period I	Calibration based on collocation in period III	Calibration based on collocation in period I	Calibration based on collocation in period III
414	5.5	1.9	13.2	4.8
624	3.1	1.6	7.3	3.9
625	2.8	1.3	6.7	3.3
626	6.8	1.3	177	3.4

measurements, and histograms of the normalized calibration errors. Table 2 reveals that calibrations based on more recent data (i.e. from the first week of period III) were more accurate, showing considerably smaller node-specific calibration errors. Specifically, both the MAE and MAnE increased by a factor of ~3 ($\pm$1.5) over a course of six weeks, and Fig. S5 and Table 2 show that the calibrations of sensors 414 and 626 were less stable than of sensors 624 and 625. In fact, this is unfortunate since, by chance, the former two sensors were involved in more re-locations during the evaluation of the N2N calibration procedure in this study.

4.4. Evaluation of node-to-node calibration

4.4.1. Collocated nodes
The MAE and MAnE of all the N2N calibration sequences are summarized in Table 3. Together, Table 3 and Figs. S6 and S7 show that N2N calibration (with up to two intermediate nodes) did not propagate considerable calibration errors (MAE $\leq$3.6 ppb and $\leq$16.1 ppb for O_3 and NO, respectively, MAnE $\leq$7.9% and $\leq$27.6% for O_3 and NO, respectively) relative to direct calibration (MAE $\leq$2.9 ppb and $\leq$16.2 ppb for O_3 and NO, respectively, MAnE $\leq$7.6% and $\leq$26% for O_3 and NO, respectively). It is noteworthy (although anecdotal) that in some cases (e.g. Set:scenario 1:2 and 4:2, Table 3) the N2N calibration with two intermediate nodes performed even better than the direct calibration. Furthermore, for the small number of nodes ($\leq$3) for which we could test the theoretical N2N calibration predictions, the experimental results of the collocation setup showed only limited sensitivity to the length of the calibration chain (Tables S1 and S2 in the SI show the effects of the N2N sequence length on the calibration parameters, $\hat{\alpha}$ and $\hat{\beta}$).

4.4.2. Field deployment
To test N2N calibration under real urban deployment conditions, we used five O_3 sensors mounted on Elm nodes to build two N2N

Table 3
MAE (ppb) and MAnE (%) of direct and N2N calibrations in the collocation experiments. (The statistics are detailed in the SI).

Experiment		MAE (MAnE)		
		Direct calibration	N2N calibration with one intermediate node	N2N calibration with two intermediate nodes
Set 1	Scenario 1 (Fig. S4a)	2.4 (7.6)	2.3 (6.9)	2.4 (7.4)
	Scenario 2 (Fig. S5a)	2.4 (7.6)	1.9 (5.8)	2.0 (6.2)
Set 2	Scenario 1 (Fig. S4c)	2.9 (6.8)	3.1 (7.1)	3.6 (7.9)
	Scenario 2 (Fig. S5c)	2.9 (6.8)	2.9 (6.8)	3.1 (6.9)
Set 3	Scenario 1 (Fig. S4b)	5.0 (26.0)	5.4 (26.1)	5.2 (25.7)
	Scenario 2 (Fig. S5b)	5.0 (26.0)	6.1 (26.6)	5.6 (26.5)
Set 4	Scenario 1 (Fig. S4d)	15.7 (21.4)	16.1 (26.9)	16.1 (27.6)
	Scenario 2 (Fig. S5d)	16.2 (21.1)	15.2 (23.4)	15.2 (22.9)

calibration sequences of length $n = 3$ (Fig. S1), and compared their results to that of the direct calibration (Fig. 5 and Table 4). Differences of MAE ≤ 2.4 ppb (MAnE $\leq 5.7\%$) between N2N calibration with two intermediate nodes and direct calibration were evident. The corresponding differences in the collocation setup (Set 1 and 2, Table 3) were MAE ≤ 0.7 ppb and MAnE $\leq 1.4\%$. Namely, for a chains of $n = 3$ O_3 sensors the differences in both MAE and MAnE between *in-situ* N2N calibrations (Table 4) and the corresponding direct calibrations (i.e. during collocation at the AQM station; Table 3) are larger by a factor of about 3. Hence, while N2N chain calibration can be applied for *in situ* calibration of deployed WDSN nodes, it does

propagate calibration errors that limit its accuracy for long chains, as was shown also in Fig. 2 (and in contrast to the results of our collocation experiment). Clearly, firmer conclusions require further testing on a larger scale. In part, our results represent the quality of the sensors used in this study (see Sensor Technologies), which affects the minimal collocation period required for reliable calibration (t_c) and the maximal time-period between consecutive calibrations (τ). With better sensors the general properties of the N2N calibration will still be valid (e.g. its dependence on the quality of individual sensors and on the length of the sensor sequence in the calibration chain) but our specific results (t_c, τ, max n before the
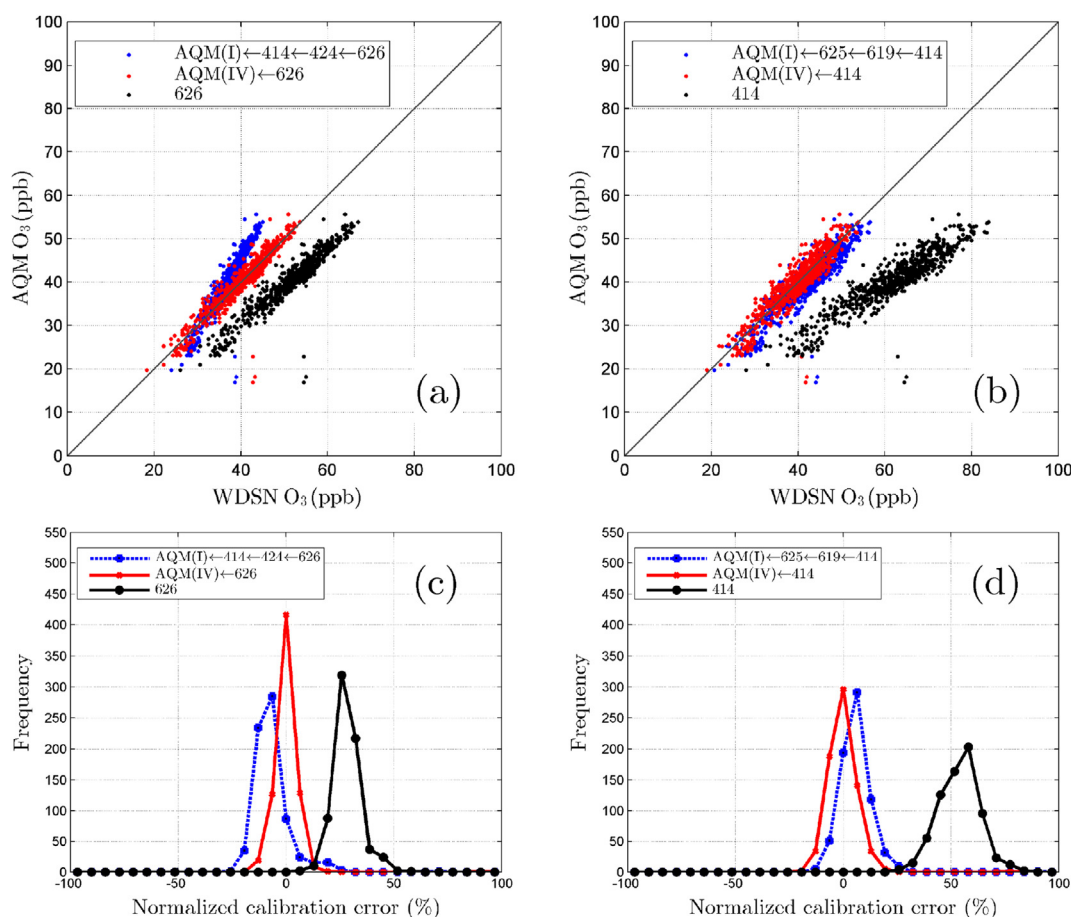

Fig. 5. Evaluation of direct and N2N calibration of O_3 Elm sensors 626 (left) and 414 (right) against AQM NSH O_3 data. Panels (a) and (b) present the scatter plots, and panels (c) and (d) present the histograms of the normalized residual errors. Black: uncalibrated data, red: directly calibrated data based on collocation during the 4th week of the experiment (see text), blue: N2N calibration with two intermediate nodes, calibration based on paired measurements from the first three weeks of the experiment and evaluation based on data from the 4th week, each pair of sensors was collocated for one week in a different location (see Fig. S1). (For interpretation of the references to colour in this figure legend, the reader is referred to the web version of this article).

Table 4
MAE (ppb) and MAnE (%) of direct and N2N chain calibrations of MO O_3 sensors mounted in WDSN nodes that were deployed in the Neve Shaanan urban neighborhood between 29/4–29/7, 2014 (Fig. 3 and Fig. S1).

	MAE (ppb)		MAnE (%)	
	Direct calibration	N2N calibration with two intermediate nodes	Direct calibration	N2N calibration with two intermediate nodes
Scenario 1	1.4	3.8	3.4	9.1
Scenario 2	1.9	2.6	4.7	6.9

normalized calibration error is larger than, e.g., 30%, etc.) may change.

In-situ N2N chain calibration has few limitations. First, if nodes are moved around deployment sites the continuity of their measurements is interrupted, yet this is also true for calibration by collocation at an AQM station. Second, N2N calibration involves accumulation of calibration errors that may result in a considerable overall calibration error as the length of the sensor chain increases. Nonetheless, using relatively short chains (in our case $n \leq 3$) enables N2N calibration with manageable calibration errors. In practice, this means that a large WDSN will require a considerable number of extra nodes to enable reliable N2N calibration. Based on our results, it seems that ~30% nodes in excess of the number of deployment sites are required for maintaining the N2N calibration process. Alternatively, instead of using identical nodes a dedicated set of high-quality nodes ("super nodes") can be used for the N2N calibration, i.e. using the super-nodes as roaming nodes. The analytical derivation of the propagation of the calibration error suggests that using such high-end nodes will reduce the overall calibration error as a result of (a) reducing the error of any individual calibration (due to the improved sensor performance), and (b) limiting the calibration chain to $n = 2$ (with $n = 1$ being the super-node). Whereas super-nodes will cost more than simple WDSN nodes, their own calibration against the AQM reference device will last longer and enable numerous pairings of the super-node and regular nodes between consecutive calibrations of the super-node (i.e. a larger τ).

5. Conclusions

We studied N2N chain calibration of WDSN sensors analytically, numerically and experimentally, and confirmed that after collocation at an AQM station convergence of the slope, intercept, and goodness of fit of the linear calibration is attained, in agreement with (Moltchanov et al., 2015). The theoretical results revealed that the length of the sensor sequence that can be used for N2N calibration strongly depend on the performance of individual sensors, as well as on the measured concentrations. In particular, the higher the ambient concentrations the more accurate the sensors are and the longer the chain that can be applied for N2N calibration while the accumulated calibration errors are still low, in accordance with (Fishbain et al., 2017). This suggests that WDSN for air quality measurements will perform better in traffic-affected inner-city sites (Castell et al., 2017), in more polluted geographical regions (e.g. megapolises in India, China, Pakistan, Nigeria, Bangladesh, etc.), and when ambient pollutant levels span a decent range that enables reliable calibration.

The experimental evaluation of N2N calibration was performed using two study designs: with the measurements collected during collocation of the nodes at AQM stations, and with the measurements collected while the nodes were deployed in an urban neighborhood, imitating an operational WDSN. We showed that a N2N calibration of individual sensors is possible, and that when the calibration is performed while the sensors are collocated at the AQM station the N2N calibration is comparable to a direct calibration. Yet, a N2N calibration during collocation has no real merit and it was examined only to gain better understanding of the propagation of calibration errors throughout the *in-situ* N2N calibration process. In general, the flexibility of N2N calibration enables more frequent calibrations of sensors that require it although, for practical reasons, we applied a uniform calibration period ($T = 7$ days) throughout the study. It is noteworthy that with current sensor technology, sensor performance must be monitored continuously on a sensor-by-sensor (rather than on a batch-by-batch) basis.

Owing to the sensor sensitivity to varying environmental conditions and to aging (drift), WDSN calibration is a major obstacle to their deployment and use. We believe that the N2N calibration scheme can provide a reasonable solution to the required frequent calibrations of WDSN nodes. We were able to test N2N calibration chains of up to three sensors, i.e. an overall calibration period of 3 weeks, which for the sensors we used is about half of the calibration persistence (τ ~6 weeks). While future improvements in sensor technology may spare the need for frequent calibrations, in the meantime *in-situ* N2N field calibration can support the spread of WDSN technology for air pollution surveillance.

Acknowledgement

Appendix A. Supplementary data

Supplementary data related to this article can be found at https://doi.org/10.1016/j.envpol.2017.09.042.

References

Balzano, L., Nowak, R., 2007. Blind calibration of sensor networks. In: Proc. 6th Int. Conf. Info. Process. Sens. Networks-IPSN '07. IEEE, pp. 79–88. http://dx.doi.org/10.1109/IPSN.2007.4379667.

Bychkovskiy, V., Megerian, S., Estrin, D., Potkonjak, M., 2003. A collaborative approach to in-place sensor calibration. In: Proceedings of the 2nd International Conference on Information Processing in Sensor Networks. Springer-Verlag Berlin, Heidelberg, pp. 301–316.

Castell, N., Dauge, F.R., Schneider, P., Vogt, M., Lerner, U., Fishbain, B., Broday, D.M., Bartonova, A., 2017. Can commercial low-cost sensor platforms contribute to air quality monitoring and exposure estimates? Env. Int. 99, 293–302.

Crouse, D.L., Peters, P.A., van Donkelaar, A., Goldberg, M.S., Villeneuve, P.J., Brion, O., Khan, S., Atari, D.O., Jerrett, M., Pope, C.A., Brauer, M., Brook, J.R., Martin, R.V., Stieb, D., Burnett, R.T., 2012. Risk of nonaccidental and cardiovascular mortality in relation to long-term exposure to low concentrations. Environ. Health Perspect. 120 (5), 708–714.

De Vito, S., Massera, E., Piga, M., Martinotto, L., Di Francia, G., 2008. On field calibration of an electronic nose for benzene estimation in an urban pollution monitoring scenario. Sensors Actuators B Chem. 129, 750–757.

Deary, M.E., Bainbridge, S.J., Kerr, A., McAllister, A., Shrimpton, T., 2016. Practicalities of mapping PM10 and PM2.5 concentrations on city-wide scales using a portable particulate monitor. Air Qual. Atmos. Heal 9 (8), 923–930.

Eitan, O., Yuval, Barchana, M., Dubnov, J., Linn, S., Carmel, Y., Broday, D.M., 2010. Spatial analysis of air pollution and cancer incidence rates in Haifa Bay. Isr. Sci.

Total Environ. 408, 4429—4439.

Fishbain, B., Moreno-Centeno, E., 2016. Self calibrated wireless distributed environmental sensory networks. Sci. Rep. 6, 24382—24392.

Fishbain, B., Lerner, U., Cole-Hunter, T., Castell-Balaguer, N., Popoola, O., Broday, D.M., Martinez-Iñiguez, T., Nieuwenhuijsen, M., Jovasevic-Stojanovic, M., Topalovic, D., Jones, R.L., Galea, K., Etzion, Y., Kizel, F., Golumbic, Y., Baram-Tsabari, A., Robinson, J., Kocman, D., Horvat, M., Svecova, V., Arpaci, A., Bartonova, A., 2017. An evaluation tool kit of air quality micro-sensing units. Sci. Tot. Env. 575, 639—648.

Hasenfratz, D., Saukh, O., Thiele, L., 2012. On-the-fly calibration of low-cost gas sensors. In: Picco, G.P., Heinzelman, W. (Eds.), Wireless Sensor Networks, EWSN 2012, Lecture Notes in Computer Science, vol. 7158. Springer-Verlag Berlin, Heidelberg, pp. 228—244.

Holstius, D.M., Pillarisetti, A., Smith, K.R., Seto, E., 2014. Field calibrations of a low-cost aerosol sensor at a regulatory monitoring site in California. Atmos. Meas. Tech. 7 (4), 1121—1131.

Jiao, W., Hagler, G., Williams, R., Sharpe, R., Brown, R., Garver, D., Judge, R., Caudill, M., Rickard, J., Davis, M., Weinstock, L., Zimmer-Dauphinee, S., Buckley, K., 2016. Community Air Sensor Network (CAIRSENSE) project: evaluation of low-cost sensor performance in a suburban environment in the southeastern United States. Atmos. Meas. Tech. 9, 5281—5292.

Kotsev, A., Schade, S., Craglia, M., Gerboles, M., Spinelle, L., Signorini, M., 2016. Next generation air quality platform: openness and interoperability for the Internet of Things. Sensors 16 (3), 403—419.

Kumar, P., Morawska, L., Martani, C., Biskos, G., Neophytou, M., Di Sabatino, S., Bell, M., Norford, L., Britter, R., 2015. The rise of low-cost sensing for managing air pollution in cities. Environ. Int. 75, 199—205.

Lepeule, J., Laden, F., Dockery, D., Schwartz, J., 2012. Chronic exposure to fine particles and mortality: an extended follow-up of the Harvard Six Cities study from 1974 to 2009. Environ. Health Perspect. 120 (7), 965—970.

Mead, M.I., Popoola, O.A.M., Stewart, G.B., Landshoff, P., Calleja, M., Hayes, M., Baldovi, J.J., McLeod, M.W., Hodgson, T.F., Dicks, J., Lewis, A., Cohen, J., Baron, R., Saffell, J.R., Jones, R.L., 2013. The use of electrochemical sensors for monitoring urban air quality in low-cost, high-density networks. Atmos. Environ. 70 (2), 186—203.

Moltchanov, S., Levy, I., Etzion, Y., Lerner, U., Broday, D.M., Fishbain, B., 2015. On the feasibility of measuring urban air pollution by wireless distributed sensor networks. Sci. Total Environ. 502, 537—547.

Myers, V., Broday, D.M., Steinberg, D.M., Yuval, Drory, Y., Gerber, Y., 2013. Exposure to particulate air pollution and long-term incidence of frailty after myocardial infarction. Ann. Epidemiol. 23 (7), 395—400.

O'Leary, B.F., Lemke, L.D., 2014. Modeling spatiotemporal variability of intra-urban air pollutants in Detroit: a pragmatic approach. Atmos. Environ. 94, 417—427.

Reggente, M., Peters, J., Theunis, J., Van Poppel, M., Rademaker, M., De Baets, B., Kumar, P., 2015. A comparison of strategies for estimation of ultrafine particle number concentrations in urban air pollution monitoring networks. Environ. Pollut. 199, 209—218.

Sampson, P.D., Richards, M., Szpiro, A.A., Bergen, S., Sheppard, L., Larson, T.V., Kaufman, J.D., 2013. A regionalized national universal kriging model using partial least squares regression for estimating annual PM2.5 concentrations in epidemiology. Atmos. Environ. 75, 383—392.

Saukh, O., Hasenfratz, D., Thiele, L., 2015. Reducing multi-hop calibration errors in large-scale mobile sensor networks. In: Proceedings of the 14th International Conference on Information Processing in Sensor Networks, pp. 274—285.

Spinelle, L., Gerboles, M., Villani, M.G., Aleixandre, M., Bonavitacola, F., 2015. Field calibration of a cluster of low-cost available sensors for air quality monitoring. Part A: ozone and nitrogen dioxide. Sensors Actuators B Chem. 215, 249—257.

Taylor, J.R., 1997. An Introduction to Error Analysis - the Study of Uncertainties in Physical Measurements, second ed. University Science Books, USA.

Whitworth, K.W., Symanski, E., Lai, D., Coker, A.L., 2011. Kriged and modeled ambient air levels of benzene in an urban environment: an exposure assessment study. Env. Heal 10, 21—31.

Williams, D., Henshaw, G., Bart, M., Laing, G., Wagner, J., Naisbitt, S., Salmond, J., 2013. Validation of low-cost ozone measurement instruments suitable for use in an air-quality monitoring network. Meas. Sci. Technol. 24 (6), 5803—5814.

World Health Organization, 2013. Review of Evidence on Health Aspects of Air Pollution — REVIHAAP Project. WHO Regional Office for Europe, Copenhagen, Denmark. http://www.euro.who.int/__data/assets/pdf_file/0004/193108/REVIHAAP-Final-technical-report-final-version.pdf?ua=1.

Yuval, Broday, D.M., 2006. High-resolution spatial patterns of long-term mean concentrations of air pollutants in Haifa Bay area. Atmos. Environ. 40 (20), 3653—3664.

Yuval, Levy, I., Broday, D.M., 2017. Improving modeled air pollution concentration maps by residual interpolation. Sci. Tot. Environ. 598, 780—788.

Zandbergen, P.A., Hart, T.C., Lenzer, K.E., Camponovo, M.E., 2012. Error propagation models to examine the effects of geocoding quality on spatial analysis of individual-level datasets. Spatial Spatiotemporal Epidemiol 3 (1), 69—82.